A doping-dependent switch from one- to two-component superfluidity at high temperatures in coupled electron-hole van der Waals heterostructures

Sara Conti[1,2], Matthias Van der Donck[2], Andrea Perali[3], Francois M. Peeters[2], and David Neilson[1,2]

[1]*Physics Div., School of Science & Technology, Università di Camerino, 62032 Camerino (MC), Italy*
[2]*Department of Physics, University of Antwerp, Groenenborgerlaan 171, B-2020 Antwerpen, Belgium*
[3]*Supernano Laboratory, School of Pharmacy, Università di Camerino, 62032 Camerino (MC), Italy*

The hunt for high temperature superfluidity has received new impetus from the discovery of atomically thin stable materials. Electron-hole superfluidity in coupled $MoSe_2$-WSe_2 monolayers is investigated using a mean-field multiband model that includes the band splitting caused by the strong spin-orbit coupling. This splitting leads to a large energy misalignment of the electron and hole bands which is strongly modified by interchanging the doping of the monolayers. The choice of doping determines if the superfluidity is tuneable from one- to two-components. The electron-hole pairing is strong, with high transition temperatures in excess of $T_c \sim 100$ K.

Recently strong signature of electron-hole superfluidity was reported in double bilayer graphene (DBG) [1], in which an n-doped bilayer graphene was placed in close proximity with a p-doped bilayer graphene, separated by a very thin insulating barrier to block recombination. The transition temperature is very low, $T_c \sim 1$ K. This can be traced back to the very strong interband screening [2] due to bilayer graphene's tiny band gap [3].

Monolayers of the Transition Metal Dichalcogenides (TMDC) MoS_2, $MoSe_2$, WS_2, and WSe_2 are semiconductors with large and direct bandgaps, $E_g \gtrsim 1$ eV [4, 5] that make interband processes and screening negligible. The effective masses in their low-lying nearly parabolic bands, are larger than in bilayer graphene, resulting also in much stronger coupling of the electron-hole pairs [6].

Because of the strong spin-orbit coupling, the heterostructure $MoSe_2$-hBN-WSe_2, with one TMDC monolayer n-doped and the other p-doped, is an interesting platform for investigating novel multicomponent effects for electron-hole superfluidity [7–9]. The hexagonal Boron Nitride (hBN) insulating layer inhibits electron-hole recombination [10], and avoids hybridization between the $MoSe_2$ and WSe_2 bands.

Table I gives the parameters for the $MoSe_2$ and WSe_2 monolayers, and Fig. 1 shows their low-lying band structures. The splitting of the conduction and valence bands by spin-orbit coupling into multibands consisting of two concentric parabolic spin-polarised subbands, makes superfluidity in double TMDC monolayers resemble high-T_c multiband superconductivity. Multiband superconductivity is emerging as a complex quantum coherent phenomenon with physical outcomes radically different, or even absent, from its single-band counterparts [11]. There are close relations with multiband superfluidity in ultracold Fermi gases [12] and with electric-field induced superconductivity at oxide surfaces [13, 14].

Table I shows that the spin splitting of the valence bands λ_v is an order of magnitude larger than the spin splitting of the conduction bands λ_c. This results in a misalignment between the electron and hole bands,
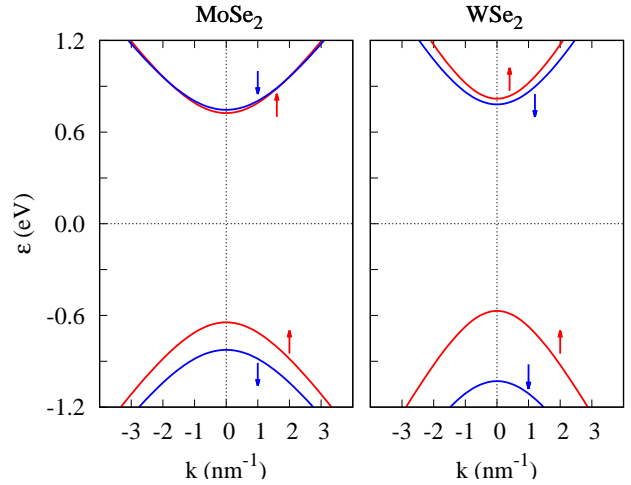

Figure 1. (Color online) The low-lying band structures of monolayer $MoSe_2$ and WSe_2 centred in the K valley. Red and blue lines are for the opposite spins. The spin configuration is opposite in the two valleys [15].

TMDC	a (nm)	t (eV)	E_g (eV)	λ_c (eV)	λ_v (eV)
$MoSe_2$	0.33	0.94	1.47	-0.021	0.18
WSe_2	0.33	1.19	1.60	0.038	0.46

Table I. TMDC monolayer lattice constant (a), hopping parameter (t), band gap (E_g), and splitting of conduction band (λ_c) and valence band (λ_v) by spin-orbit coupling [15–17].

as shown in Fig. 2. (For the p-doped monolayer, we are using the standard particle-hole mapping of the valence band to a conduction band, with positively charged holes filling conduction band states up to the Fermi level. Thanks to the large band gaps, we only need to consider conduction band processes [2, 18].) A Coulomb pairing interaction, in contrast with conventional BCS pairing, has no dependence on the electron and hole spins. Therefore for each monolayer, we label the bottom and top conduction subbands by $\beta = b$ and $\beta = t$. Due to the large valley separation in momentum space, interval-
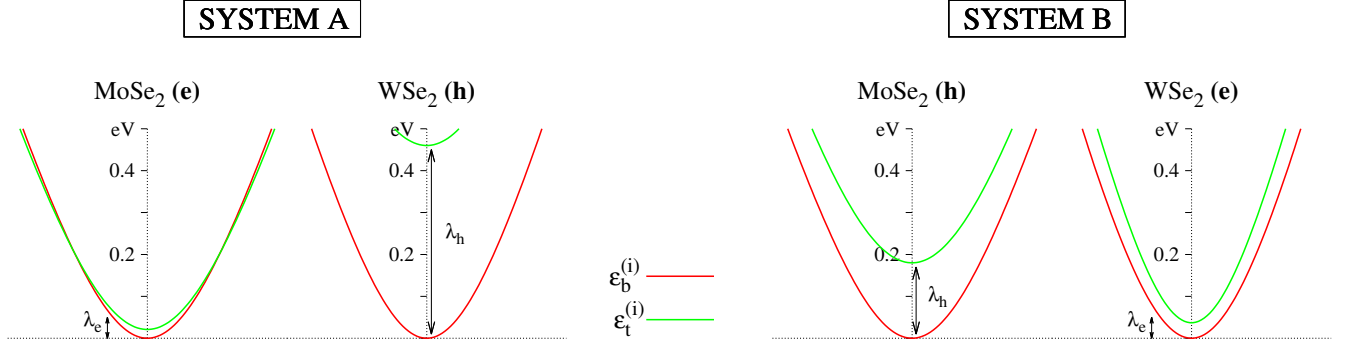
Figure 2. (Color online) Subbands of systems A and B (see text) centred in the K valley. For the p-doped monolayer, the valence band has been mapped into a conduction band using the standard particle-hole transformation. The bottom electron $\varepsilon_b^e(k)$ and hole $\varepsilon_b^h(k)$ subbands have been aligned. Zero energy is set at $\varepsilon_b^e(k=0)$.

ley scattering is negligible, so the effect of the two valleys appears only in a valley degeneracy factor, $g_v = 2$.

We will find the misalignment strongly affects the electron-hole pairing processes, and that due to the very different misalignments of the bands (Fig. 2), the n-doped-MoSe$_2$ with p-doped-WSe$_2$ (denoted as system A) has markedly different properties from the p-doped-MoSe$_2$ with n-doped-WSe$_2$ (system B).

The multiband electron-hole Hamiltonian is,

$$
\begin{aligned}
H = \sum_{k,\beta} &\left\{ \xi_\beta^{(e)}(k)\, c_{\beta,k}^\dagger\, c_{\beta,k} + \xi_\beta^{(h)}(k)\, d_{\beta,k}^\dagger\, d_{\beta,k} \right\} \\
&+ \sum_{\substack{k,k',q \\ \beta,\beta'}} V_{k\,k'}^D\, c_{\beta,k+q/2}^\dagger\, d_{\beta,-k+q/2}^\dagger\, c_{\beta',k'+q/2}\, d_{\beta',-k'+q/2}
\end{aligned}
\tag{1}
$$

For the n-doped monolayer, $c_{\beta,k}^\dagger$ and $c_{\beta,k}$ are the creation and annihilation operators for electrons in conduction subband β, while for the p-doped monolayer, $d_{\beta,k}^\dagger$ and $d_{\beta,k}$ are the corresponding operators for holes. The kinetic energy terms are $\xi_\beta^{(i)}(k) = \varepsilon_\beta^{(i)}(k) - \mu^{(i)}$ where $\varepsilon_\beta^{(i)}(k)$ is the energy dispersion for the $i = e, h$ monolayer [19]. Because of the small difference between electron and hole effective masses, we assume bands of the same curvature, and so since we consider only equal carrier densities $n^e = n^h = n$, for the chemical potentials $\mu^{(e)} = \mu^{(h)} \equiv \mu$. $V_{k\,k'}^D$ is the bare attractive Coulomb interaction between electrons and holes in opposite monolayers separated by a barrier of thickness d,

$$
V_{k\,k'}^D = -V_{k\,k'}^S e^{-d|\mathbf{k}-\mathbf{k}'|} \;, \quad V_{k\,k'}^S = \frac{2\pi e^2}{\epsilon}\frac{1}{|\mathbf{k}-\mathbf{k}'|} \;, \tag{2}
$$

where $V_{k\,k'}^S$ is the bare repulsive Coulomb interaction be-

tween carriers in the same monolayer.

In principle there are four possible electron-hole pairings, corresponding to four superfluid condensates [20] $\{\beta\beta'\}$. The first index β refers to the electron subbands and the second β' to the hole subbands. We find that the $\{bt\}$ and $\{tb\}$ cross-pairing make negligible contributions to the condensates, so for simplicity, we confine our attention to the mean-field equations for the superfluid gaps $\Delta_{bb}(k)$ and $\Delta_{tt}(k)$. Since there are no spin-flip scattering processes, Josephson-like pair transfer is forbidden. At zero temperature these gap equations are (see Appendix),

$$
\Delta_{bb}(k) = -\frac{1}{L^2}\sum_{k'} F_{kk'}^{bb}\, V_{k\,k'}^{eh}\, \frac{\Delta_{bb}(k')}{2E_b(k')} \quad , \tag{3}
$$

$$
\Delta_{tt}(k) = -\frac{1}{L^2}\sum_{k'} F_{kk'}^{tt}\, V_{k\,k'}^{eh}\, \frac{\Delta_{tt}(k')}{2E_t(k')}\theta[E_t^-(k')] \;. \tag{4}
$$

$E_\beta(k) = \sqrt{\xi_\beta(k)^2 + \Delta_{\beta\beta}^2(k)}$ is the quasi-particle excitation energy for subband β, with $\xi_\beta(k) = (\xi_\beta^{(e)} + \xi_\beta^{(h)})/2$. $E_t^\pm(k) = E_t(k) \pm \delta\lambda$ with $\delta\lambda = (\lambda_h - \lambda_e)/2$. λ_h is the spin-splitting of the conduction band of the p-doped monolayer, and λ_e the corresponding spin-splitting for the n-doped monolayer, with values taken from Table I. $\theta[E_t^-(k)] = 1 - f[E_t^-(k), 0]$ is a step function associated with the zero temperature Fermi-Dirac distribution. $F_{kk'}^{\beta\beta} = |\langle \beta k\,|\,\beta k'\rangle|^2$ is the form factor that accounts for the overlap of single-particle states in k and k' for subbands β in opposite monolayers [21] (see Appendix).

$V_{kk'}^{eh}$ in Eqs. (3-4) is the screened electron-hole interaction. We use the linear-response random phase approximation for static screening in the superfluid state [2],

$$
V_{k\,k'}^{eh} = \frac{V_{k\,k'}^D + \Pi_a(q)[(V_{k\,k'}^S)^2 - (V_{k\,k'}^D)^2]}{1 - 2[V_{k\,k'}^S\Pi_n(q) + V_{k\,k'}^D\Pi_a(q)] + [\Pi_n^2(q) - \Pi_a^2(q)][(V_{k\,k'}^S)^2 - (V_{k\,k'}^D)^2]} \;, \tag{5}
$$

where $q = |\mathbf{k} - \mathbf{k}'|$. $\Pi_n(q)$ is the normal polarizability in the superfluid state and $\Pi_a(q)$ is the anomalous polarizability [22, 23], which is only non-zero in the superfluid state. $\Pi_n(q)$ depends on the population of free carriers (see Appendix). $\Pi_a(q)$, with opposite sign, depends on the population of electron-hole pairs. The combined effect of $\Pi_n(q)$ and $\Pi_a(q)$ is that a large superfluid condensate fraction of strong-coupled and approximately neutral pairs is associated with very weak screening [24]. This is because of the small remaining population of charged free carriers available for screening.

Equation (3) has the same form as for a decoupled one-band system,because the two b bands are aligned [25]. In contrast, Eq. (4) shows explicitly the effect of misalignment of the t bands (Fig. 2) through the term $\theta[E_t^-(k')] \equiv \theta[\sqrt{\xi_t(k)^2 + \Delta_{tt}^2(k)} - \delta\lambda]$. This can only drop below unity at higher densities where the pair coupling strength is weak compared with the misalignment.

For a given chemical potential μ, the carrier density n of one monolayer is determined as a sum of the subband carrier densities n_b and n_t by,

$$n = g_s g_v \sum_{\beta=b,t} n_\beta \qquad (6)$$

$$n_b = \frac{1}{L^2} \sum_k v_b^2(k) \qquad (7)$$

$$n_t = \frac{1}{L^2} \sum_k v_t^2(k)\theta[E_t^+(k)] + u_t^2(k)(1 - \theta[E_t^-(k)]) \qquad (8)$$

where v_β^2 and u_β^2 are the Bogoliubov amplitudes for the subbands β (see Appendix). Because of the spin polarisation in the valleys, the spin degeneracy is $g_s = 1$.

The regimes of the superfluid crossover are characterized by the superfluid condensate fraction C [26, 27]. C is defined as the fraction of carriers bound in pairs relative to the total number of carriers. For $C > 0.8$ the condensate is in the strong-coupled BEC regime, for $0.2 \le C \le 0.8$ in the crossover regime, and for $C < 0.2$ in the BCS regime. In our system, the two condensate fractions are given by,

$$C_{\beta\beta} = \frac{\sum_k u_\beta^2(k)\, v_\beta^2(k)}{\sum_k v_\beta^2(k)}. \qquad (9)$$

Figure 3(b) shows the dependence on WSe$_2$ electron density of the maximum of the superfluid gaps $\Delta_{\beta\beta} = \max_k \Delta_{\beta\beta}(k)$ for the b and t bands (Eqs. (3-4)) in systems A and B. We took equal effective masses $m_e^* = m_h^* = 0.44m_e$, a barrier thickness $d = 1$ nm, and dielectric constant $\epsilon = 2$, for monolayers encapsulated in few layers of hBN [28].

Figure 3(c) shows the evolution of the condensate fractions (Eq. (9)) as a function of density, and Fig. 3(a) the evolution of the chemical potential.

We see in Fig. 3(b) that the form of Δ_{bb} is similar for systems A and B. At low densities the system is in
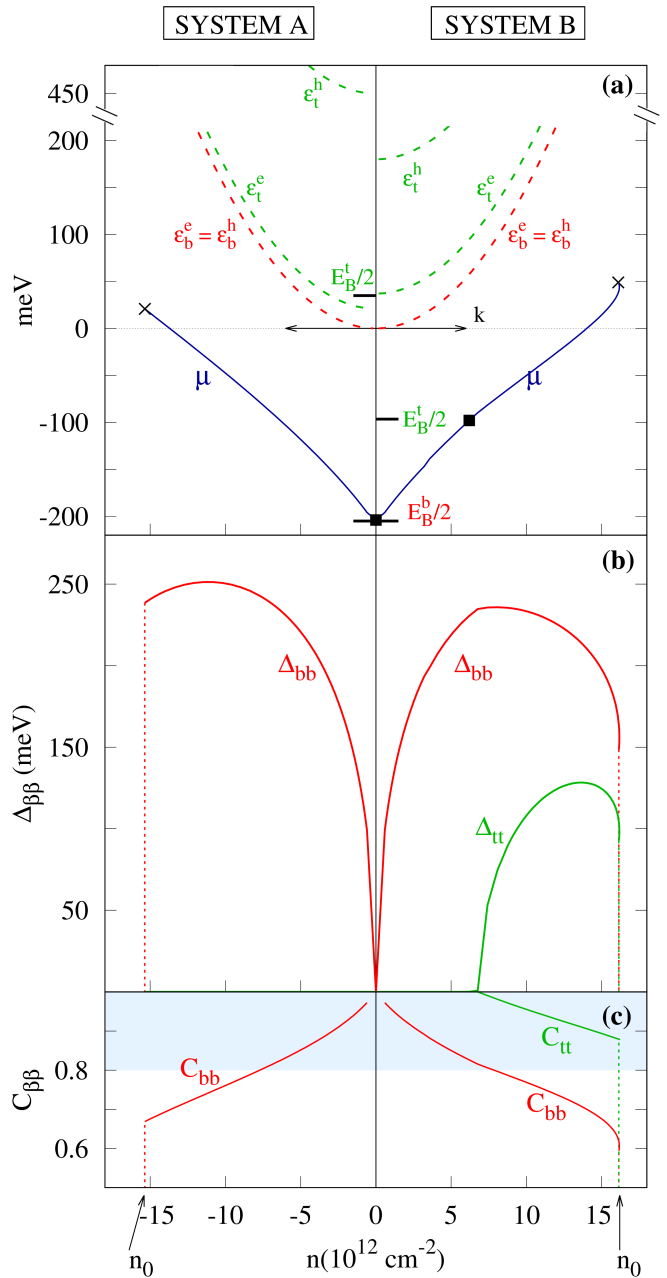

Figure 3. (Color online) (a) Chemical potential as function of density n of WSe$_2$. Positive density corresponds to system A, negative density to system B. For reference, the energy bands are shown as a function of k with the same energy scale. The bound state energies $E_B^b/2$, $E_B^t/2$ are also indicated with respect to the bands. (b) The maximum of the superfluid gaps Δ_{bb} Δ_{tt} as a function of n. (c) Corresponding condensate fraction C_{bb} and C_{tt}. The blue shaded area is the BEC regime.

the strong coupled BEC regime, with condensate fraction $C_{bb} > 0.8$. At these densities the $\{bb\}$ pairing is to a deep bound state with binding energy $E_B^b \sim 400$ meV below the bottom of the b band [29, 30] . The chemical potential is $\mu \sim -E_B^b/2$ (Fig. 3(a)). With increasing density, Δ_{bb} increases and then passes through a maximum. μ also

increases and approaches zero. Eventually, Δ_{bb} drops sharply to zero at a superfluid threshold density n_0. For $n > n_0$, the screening of the pairing interaction is so strong that it kills superfluidity [23].

In contrast, Δ_{tt} is only non-zero in system B. At low density, $\Delta_{tt} = 0$ also in system B, since the pairing population is zero. This is because the chemical potential μ at these densities lies below the isolated bound state associated with the t bands, located at energy $E_B^t = E_B^b - (\lambda_e + \lambda_h)$. It is only when μ passes above $-E_B^t/2$ that this state can be populated, so Δ_{tt} can become non-zero. Further increasing the density increases the $\{tt\}$ pair population, Δ_{tt} increases and then passes through a maximum. When μ becomes positive, the build up of free carriers, as evidenced by $C_{bb} < 0.8$ in Fig. 3(c), combined with the misalignment of the t bands, starts to significantly weaken the effective electron-hole screened interaction. Eventually screening kills the superfluidity in both $\{bb\}$ and $\{tt\}$ channels at the same threshold density.

We see in Fig. 3(b) that the behavior of Δ_{tt} in systems A and B is completely different. In system A the chemical potential remains below the isolated bound state E_B^t associated with the t bands over the full range of densities up to n_0. With μ lying below E_B^t, the population of pairs in the $\{tt\}$ channel remains zero. The only difference between system A and B is the choice of doping which results in the markedly different misalignment of the t bands, leading to one-component or two-components superfluidity.

In Fig. 3(c), we note that the threshold densities n_0 for the superfluidity are much larger than the threshold densities $n_0 \sim 8 \times 10^{11}$ cm^{-2} in double bilayer graphene [1, 2], and the $n_0 \sim 4 \times 10^{12}$ cm^{-2} predicted for double layer phosphorene [31]. n_0 is large for the double TMDC monolayers for two main reasons: (i) the large effective masses of the electrons and holes means a large effective Rydberg energy scale, thus large superfluid gaps Δ that strongly suppress the screening; (ii) the large TMDC monolayer bandgaps E_g eliminate valence band screening, making the electron-hole pairing interaction very strong [2].

These large threshold densities in the double TMDC monolayers lead to high Berezinskii-Kosterlitz-Thouless transition temperatures T_{KT} [32]. The monolayers have near parabolic bands, so we can approximate [33, 34],

$$T_{KT} = \frac{\pi}{2}\rho_s(T_{KT}) \simeq n\, \frac{\pi\hbar^2}{8g_s g_v m^*} \ . \qquad (10)$$

$\rho_s(T)$ is the superfluid stiffness. Equation (10) gives transition temperatures for systems A and B at their threshold densities of $T_{KT}^A = 110$ K and $T_{KT}^B = 120$ K.

The strikingly different behavior of Δ_{tt} in the two systems is a new and remarkable effect that can be probed using angle-resolved photoemission spectroscopy (ARPES) [35]. ARPES measures the spectral function, which in a one-component superfluid state like system A will have a single peak centred at a negative frequency corresponding to Δ_{bb}. However in system B, when it switches from one-component to two-components superfluidity, two peaks associated with the gaps Δ_{bb} and Δ_{tt} will appear in the spectral function at negative frequencies [36]. Other experimental techniques that can be used to detect the presence or absence of the second gap Δ_{tt} are Andreev reflection spectroscopy [37, 38] and scanning tunneling microscopy (STM) [39].

The large gaps at zero temperature and in the BCS-BEC crossover regime should lead to pseudogaps in the single-particle excitation spectra [40] above T_{KT}, that persist up to temperatures of the order of the zero temperature gaps. These could also be detected by theARPES and STM. System B at densities where both the superfluid components are close to their maximum gaps would favour large pseudogaps, while configurations with one large gap and one small or zero gap would lead to screening of superfluid fluctuations and suppression of the pseudogap [41].

In summary, we have investigated multicomponent effects for electron-hole multiband superfluidity in n-p and p-n doped MoSe$_2$-hBN-WSe$_2$ heterostructures (systems A and B, respectively). Both systems are multiband and can stabilize electron-hole superfluidity at temperatures above 100 K.

Surprisingly we find that only in system B can superfluidity have two components. For both systems we would have expected to be able to tune from one- to two-component superfluidity by increasing the density, as recently observed in multiband superconductors [14], and this is indeed the case for system B. However for system A, the very large misalignment of the electron and hole top bands, means that there are no carriers available for pairing in the topmost band before screening has become so strong that it completely suppresses superfluidity. Therefore only one-component superfluidity is possible in system A. This is a remarkable result: activation of the second-component of the superfluidity in this heterostructure depends crucially on the choice of which TMDC monolayer is n-doped and which p-doped.

After completion of this paper we became aware of a recent experiment on MoSe$_2$-WSe$_2$ where exciton condensation with high transition temperatures above 100 K consistent with our predictions were reported.

Appendix: Mean field equations

To describe our system we introduce the temperature dependent normal and anomalous multiband Matsubara Green functions, with subband indices α and β,

$$\begin{cases} \mathcal{G}^{\alpha\beta}(k,\tau) &= - < Tc_k^\alpha(\tau)c_k^{\beta\dagger}(0) > \\ \mathcal{F}^{\alpha\beta}(k,\tau) &= - < Tc_k^\alpha(\tau)d_k^\beta(0) > . \end{cases} \quad (11)$$

The mean field equations for the gaps and the densities are[20]:

$$\Delta_{\alpha\beta}(k) = -\frac{T}{L^2} \sum_{\substack{\alpha',\beta', \\ k',i\omega_n}} F_{kk'}^{\alpha\beta\alpha'\beta'} V_{k\,k'}^{eh} \mathcal{F}^{\alpha'\beta'}(k',i\omega_n) \quad (12)$$

$$n_{\alpha\beta} = \frac{T}{L^2} \sum_{k,i\omega_n} \mathcal{G}^{\alpha\beta}(k,i\omega_n) \quad (13)$$

where $F_{kk'}^{\alpha\beta\alpha'\beta'} = \langle \alpha'k' \,|\, \alpha k \rangle \langle \beta k \,|\, \beta'k' \rangle$ is the form factor representing the overlap of the single particle wave functions. On the right hand side of Eq. 12, the gaps $\Delta_{\alpha\beta}(k)$ appear implicitly in the $\mathcal{F}^{\alpha\beta}$.

Since we are neglecting the cross-pairing contributions, we retain the Green functions and the form factors only for $\alpha = \beta(\alpha' = \beta')$. The screened Coulomb interaction $V_{k\,k'}^{eh}$ conserves the spin of the electron-hole pair and there are no spin-flip scattering processes implying $F_{kk'}^{\beta\beta\beta'\beta'} = 0$ for $\beta \neq \beta'$, so Josephson-like pair transfers are forbidden. The resulting gap equations are thus decoupled. For brevity, we adopt the notation $F_{kk'}^{\beta\beta\beta'\beta'} \equiv F_{kk'}^{\beta\beta'}$.

In terms of Bogoliubov amplitudes:

$$v_\beta^2(k) = \frac{1}{2}\left(1 - \frac{\xi_\beta(k)}{E_\beta(k)}\right); u_\beta^2(k) = \frac{1}{2}\left(1 + \frac{\xi_\beta(k)}{E_\beta(k)}\right), \quad (14)$$

Eqs. (11) become

$$\mathcal{G}^{\beta\beta}(k,i\omega_n) = \frac{u_\beta^2}{i\omega_n - E_\beta^-} + \frac{v_\beta^2}{i\omega_n + E_\beta^+} \quad (15)$$

$$\mathcal{F}^{\beta\beta}(k,i\varepsilon_n) = \frac{u_\beta v_\beta}{i\omega_n - E_\beta^-} + \frac{u_\beta v_\beta}{i\omega_n + E_\beta^+}, \quad (16)$$

with $E_\beta^\pm$ defined in the main manuscript.

Performing the summation over the Matsubara frequencies $\omega_n = \pi T(2n + 1)$ in the limit of zero temperature, we obtain the gap equations (Eqs. (3-4)) and the density equations (Eqs. (7-8)) in the main manuscript.

The polarizabilities in the presence of the superfluid are [22]:

$$\Pi_n(q,\Omega_l) = T\frac{g_s g_v}{L^2} \sum_{\beta,k',i\omega_n} F_{kk'}^{\beta\beta} \mathcal{G}^{\beta\beta}(k',i\omega_n+i\Omega_l)\mathcal{G}^{\beta\beta}(k,i\omega_n) \quad (17)$$

$$\Pi_a(q,\Omega_l) = T\frac{g_s g_v}{L^2} \sum_{\beta,k',i\omega_n} F_{kk'}^{\beta\beta} \mathcal{F}^{\beta\beta}(k',i\omega_n+i\Omega_l)\mathcal{F}^{\beta\beta}(k,i\omega_n) \quad (18)$$

where $q = |\mathbf{k} - \mathbf{k'}|$. The polarizabilities in the effective electron-hole interaction (Eq. (5) in the main manuscript) are obtained by evaluating Eqs. (17) and (18) at zero temperature in the static limit, $\Omega_l \to 0$.

[1] G. W. Burg, N. Prasad, K. Kim, T. Taniguchi, K. Watanabe, A. H. MacDonald, L. F. Register, and E. Tutuc, "Strongly enhanced tunneling at total charge neutrality in double-bilayer graphene-WSe₂ heterostructures," Phys. Rev. Lett. 120, 177702 (2018).

[2] S. Conti, A. Perali, F. M. Peeters, and D. Neilson, "Multicomponent screening and superfluidity in gapped electron-hole double bilayer graphene with realistic bands," Phys. Rev. B 99, 144517 (2019).

[3] Y. Zhang, T. T. Tang, C. Girit, Z. Hao, M. C. Martin, A. Zettl, M. F. Crommie, Y. R. Shen, and F. Wang, "Direct observation of a widely tunable bandgap in bilayer graphene," Nature (London) 459, 820 (2009).

[4] K. F. Mak, C. Lee, J. Hone, J. Shan, and T. F. Heinz, "Atomically thin MoS₂: a new direct-gap semiconductor," Phys. Rev. Lett. 105, 136805 (2010).

[5] H. Jiang, "Electronic band structures of molybdenum and tungsten dichalcogenides by the GW approach," J. Phys. Chem. C 116, 7664 (2012).

[6] M. M. Fogler, L. V. Butov, and K. S. Novoselov, "High-temperature superfluidity with indirect excitons in van der Waals heterostructures," Nat. Commun. 5, 4555 (2014).

[7] P. Rivera, J. R. Schaibley, A. M. Jones, J. S. Ross, S. Wu, G. Aivazian, P. Klement, K. Seyler, G. Clark, N. J. Ghimire, et al., "Observation of long-lived interlayer excitons in monolayer MoSe₂-WSe₂ heterostructures," Nat. Commun. 6, 6242 (2015).

[8] S. Ovesen, S. Brem, C. Linderälv, M. Kuisma, T. Korn, P. Erhart, M. Selig, and E. Malic, "Interlayer exciton dynamics in van der waals heterostructures," Communications Physics 2, 23 (2019).

[9] M. Förg, L. Colombier, R. K. Patel, J. Lindlau, A. D Mohite, H. Yamaguchi, M. M. Glazov, D. Hunger, and A. Högele, "Cavity-control of interlayer excitons in van der Waals heterostructures," Nat. Commun. 10, 3697 (2019).

[10] L. Britnell, R. V. Gorbachev, R. Jalil, B. D. Belle, F. Schedin, M. I. Katsnelson, L. Eaves, S. V. Morozov, A. S. Mayorov, N. MR. Peres, A. H. Castro Neto, J. Leist, A. K. Geim, L. A. Ponomarenko, and K. S. Novoselov, "Electron tunneling through ultrathin Boron Nitride crystalline barriers," Nano Lett. 12, 1707 (2012).

[11] A. Bianconi, "Quantum materials: Shape resonances in superstripes," Nat. Phys. 9, 536 (2013).

[12] A. A. Shanenko, M. D. Croitoru, A. V. Vagov, V. M. Axt, A. Perali, and F. M. Peeters, "Atypical BCS-BEC crossover induced by quantum-size effects," Phys. Rev. A 86, 033612 (2012).

[13] Y. Mizohata, M. Ichioka, and K. Machida, "Multiple-gap structure in electric-field-induced surface supercon-

ductivity," Phys. Rev. B **87**, 014505 (2013).

[14] G. Singh, A. Jouan, G. Herranz, M. Scigaj, F. Sánchez, L. Benfatto, S. Caprara, M. Grilli, G. Saiz, F. Couëdo, C. Feuillet-Palma, J. Lesueur, and N. Bergeal, "Gap suppression at a Lifshitz transition in a multi-condensate superconductor," Nature Materials **18**, 948 (2019).

[15] D. Xiao, G. B. Liu, W. Feng, X. Xu, and W. Yao, "Coupled spin and valley physics in monolayers of MoS_2 and other group-VI dichalcogenides," Phys. Rev. Lett. **108**, 196802 (2012).

[16] Z. Y. Zhu, Y. C. Cheng, and U. Schwingenschlögl, "Giant spin-orbit-induced spin splitting in two-dimensional transition-metal dichalcogenide semiconductors," Phys. Rev. B **84**, 153402 (2011).

[17] K. Kośmider, J. W. González, and J. Fernández-Rossier, "Large spin splitting in the conduction band of transition metal dichalcogenide monolayers," Phys. Rev. B **88**, 245436 (2013).

[18] S. Conti, A. Perali, F. M. Peeters, and D. Neilson, "Multicomponent electron-hole superfluidity and the BCS-BEC crossover in double bilayer graphene," Phys. Rev. Lett. **119**, 257002 (2017).

[19] M. Van der Donck and F. M. Peeters, "Interlayer excitons in transition metal dichalcogenide heterostructures," Phys. Rev. B **98**, 115104 (2018).

[20] A. A. Shanenko, J. A. Aguiar, A. Vagov, M. D. Croitoru, and M. V. Milošević, "Atomically flat superconducting nanofilms: multiband properties and mean-field theory," Supercond. Sci. Tech. **28**, 054001 (2015).

[21] Y. E Lozovik and A. A. Sokolik, "Multi-band pairing of ultrarelativistic electrons and holes in graphene bilayer," Phys. Rev. A **374**, 326 (2009).

[22] Y. E. Lozovik, S. L. Ogarkov, and A. A. Sokolik, "Condensation of electron-hole pairs in a two-layer graphene system: Correlation effects," Phys. Rev. B **86**, 045429 (2012).

[23] A. Perali, D. Neilson, and A. R. Hamilton, "High-temperature superfluidity in double-bilayer graphene," Phys. Rev. Lett. **110**, 146803 (2013).

[24] D. Neilson, A. Perali, and A. R. Hamilton, "Excitonic superfluidity and screening in electron-hole bilayer systems," Phys. Rev. B **89**, 060502 (2014).

[25] F. G. Kochorbe and M. E. Palistrant, "Superconductivity in a two-band system with low carrier density," J. Exp. Theor. Phys. **77**, 442 (1993).

[26] L. Salasnich, N. Manini, and A. Parola, "Condensate fraction of a Fermi gas in the BCS-BEC crossover," Phys. Rev. A **72**, 023621 (2005).

[27] P. López Ríos, A. Perali, R. J. Needs, and D. Neilson, "Evidence from quantum Monte Carlo simulations of large-gap superfluidity and BCS-BEC crossover in double electron-hole layers," Phys. Rev. Lett. **120**, 177701 (2018).

[28] P. Kumar, Y. S. Chauhan, A. Agarwal, and S. Bhowmick, "Thickness and stacking dependent polarizability and dielectric constant of graphene–hexagonal boron nitride composite stacks,"

[29] M. Randeria, J.-M. Duan, and L.-Y. Shieh, "Superconductivity in a two-dimensional Fermi gas: Evolution from Cooper pairing to Bose condensation," Phys. Rev. B **41**, 327 (1990).

[30] F. Pistolesi and G. C. Strinati, "Evolution from BCS superconductivity to Bose condensation: Role of the parameter $k_F \xi$," Phys. Rev. B **49**, 6356 (1994).

[31] S. Saberi-Pouya, M. Zarenia, A. Perali, T. Vazifehshenas, and F. M. Peeters, "High-temperature electron-hole superfluidity with strong anisotropic gaps in double phosphorene monolayers," Phys. Rev. B **97**, 174503 (2018).

[32] J. M. Kosterlitz and D. J. Thouless, "Ordering, metastability and phase transitions in two-dimensional systems," J. Phys. C: Solid State **6**, 1181 (1973).

[33] L. Benfatto, M. Capone, S. Caprara, C. Castellani, and C. Di Castro, "Multiple gaps and superfluid density from interband pairing in a four-band model of the iron oxypnictides," Phys. Rev. B **78**, 140502 (2008).

[34] S. S. Botelho and C. A. R. Sá de Melo, "Vortex-antivortex lattice in ultracold fermionic gases," Phys. Rev. Lett. **96**, 040404 (2006).

[35] S. Rist, A. A. Varlamov, A. H. MacDonald, R. Fazio, and M. Polini, "Photoemission spectra of massless Dirac fermions on the verge of exciton condensation," Phys. Rev. B **87**, 075418 (2013).

[36] H. Miao, P. Richard, Y. Tanaka, K. Nakayama, T. Qian, K. Umezawa, T. Sato, Y.-M. Xu, Y. B. Shi, N. Xu, X.-P. Wang, P. Zhang, H.-B. Yang, Z.-J. Xu, J. S. Wen, G.-D. Gu, X. Dai, J.-P. Hu, T. Takahashi, and H. Ding, "Isotropic superconducting gaps with enhanced pairing on electron fermi surfaces in $FeTe_{0.55}Se_{0.45}$," Phys. Rev. B **85**, 094506 (2012).

[37] D. Daghero, P. Pecchio, G. A. Ummarino, F. Nabeshima, Y. Imai, A. Maeda, I. Tsukada, S. Komiya, and R. S. Gonnelli, "Point-contact Andreev-reflection spectroscopy in Fe (Te, Se) films: multiband superconductivity and electron-boson coupling," Supercond. Sci. Tech. **27**, 124014 (2014).

[38] T. E. Kuzmicheva, S. A. Kuzmichev, A. V. Sadakov, A. V. Muratov, A. S. Usoltsev, V. P. Martovitsky, A. R. Shipilov, D. A. Chareev, E. S. Mitrofanova, and V. M. Pudalov, "Direct evidence of two superconducting gaps in $FeSe_{0.5}$ $Te_{0.5}$: n-Andreev spectroscopy and the lower critical field," JETP Lett. **104**, 852 (2016).

[39] J. X. Yin, Z. Wu, J. H. Wang, Z. Y. Ye, J. Gong, X. Y. Hou, L. Shan, A. Li, X. J. Liang, X. X. Wu, *et al.*, "Observation of a robust zero-energy bound state in iron-based superconductor Fe (Te, Se)," Nat. Phys. **11**, 543 (2015).

[40] A. Perali, P. Pieri, G. C. Strinati, and C. Castellani, "Pseudogap and spectral function from superconducting fluctuations to the bosonic limit," Phys. Rev. B **66**, 024510 (2002).

[41] L. Salasnich, A. A. Shanenko, A. Vagov, J. Albino Aguiar, and A. Perali, "Screening of pair fluctuations in superconductors with coupled shallow and deep bands: A route to higher-temperature superconductivity," Phys. Rev. B **100**, 064510 (2019).

J. Phys. Chem. C **120**, 17620 (2016).